Final-state interactions in semi-inclusive deep inelastic scattering off the deuteron

W. Cosyn* and M. Sargsian
Department of Physics, Florida International University, Miami, Florida 33199, USA
(Received 22 February 2011; revised manuscript received 12 April 2011; published 6 July 2011)

Semi-inclusive deep inelastic scattering off the deuteron with production of a slow nucleon in recoil kinematics is studied in the virtual nucleon approximation, in which the final-state interaction (FSI) is calculated within generalized eikonal approximation. The cross section is derived in a factorized approach, with a factor describing the virtual photon interaction with the off-shell nucleon and a distorted spectral function accounting for the final-state interactions. One of the main goals of the study is to understand how much the general features of the diffractive high-energy soft rescattering accounts for the observed features of FSI in deep inelastic scattering (DIS). Comparison with the Jefferson Lab data shows good agreement in the covered range of kinematics. Most importantly, our calculation correctly reproduces the rise of the FSI in the forward direction of the slow nucleon production angle. By fitting our calculation to the data we extracted the W and Q^2 dependencies of the total cross section and slope factor of the interaction of DIS products, X, off the spectator nucleon. This analysis shows the XN-scattering cross section rising with W and decreasing with an increase of Q^2. Finally, our analysis points at a largely suppressed off-shell part of the rescattering amplitude.

DOI: 10.1103/PhysRevC.84.014601 PACS number(s): 11.80.−m, 13.60.−r, 13.85.Ni

I. INTRODUCTION

In recent years, a process that has garnered a fair amount of attention is the $^2\mathrm{H}(e, e' p_s)X$ reaction at high Q^2. In this reaction, deep inelastic scattering (DIS) occurs on a constituent of the deuteron and a slow spectator proton is detected in coincidence with the scattered electron. This reaction can be used in several ways to study the role of the QCD dynamics at nucleonic length scales. At very small spectator proton momenta, the DIS occurs on a nearly on-shell neutron and it allows one to extract information about the "free" neutron structure function F_{2N} in a way that minimizes the nuclear effects inherent to a bound neutron. Detailed information about the neutron structure function helps to constrain the QCD models of the nucleon and can be used to determine the relative d to u quark densities at large Bjorken x. At larger spectator momenta, high-density configurations of the deuteron will occur in which the proton and neutron are in very close proximity to each other. Under these circumstances the partonic structure of nucleons could strongly modify [1] with the possibility of two nucleons merging into six quark configurations at asymptotically large relative momenta in the deuteron [2,3]. Consequently, experiments that explore these kinematics can be used to study the modifications of nucleon properties and the role of quark degrees of freedom in these situations. Two recent Jefferson Lab Hall B (JLab) experiments have studied the $^2\mathrm{H}(e, e' p_s)X$ reactions: one at high [4] and the other at low spectator momenta [5]. New measurements will be possible after the 12 GeV upgrade of JLab is completed.

In experiments exploring the partonic structure of the nucleon, one generally wants to have kinematics that minimize the final-state interactions (FSI) of the produced X states with the spectator nucleon as this FSI make the extraction of the observable one is looking for less straightforward. On the other hand, the $^2\mathrm{H}(e, e' p_s)X$ reaction in kinematics that favor larger contributions from FSI can be used in order to study the process of hadronization. The attenuation of the produced hadronic state by the spectator when compared to the free process can yield information on the space-time structure of the hadronization process. Thus in this respect FSI becomes very important part of the semi-inclusive DIS process. To quantify the effects of FSI in DIS, model calculations are needed and this has already resulted in the development of several theoretical approaches [1,6–12].

The major problem one faces in calculations of FSI of DIS products with the spectator nucleon in $^2\mathrm{H}(e, e' N)X$ reactions is the lack of the detailed understanding of the composition and space-time evolution of the hadronic system produced after the deep inelastic scattering of the virtual photon off the bound nucleon. Moreover, both the composition and space-time evolution are function of the Bjorken x and Q^2 probed in the reaction.

In this paper we study the question on how much the final-state interaction of the DIS products are defined by the general properties of soft reinteractions. In other words, how far we can go with the description of FSI without knowing the specific properties of the hadronic intermediate state after the initial DIS scattering? Based on the general properties of the reaction a factorized approach is used in the calculations, whereby the cross section is split into the parts describing the interaction of the virtual photon with a bound nucleon and the distorted spectral function which includes the effect of final-state interactions. The deep inelastic interaction with moving bound nucleon is calculated within the virtual nucleon approximation while the FSI are included using the framework of generalized eikonal approximation (GEA) [13–15].

The paper is organized as follows. In Sec. II we describe the general properties of the reaction and main assumptions based

*On leave form: Department of Physics and Astronomy, Ghent University, Proeftuinstraat 86, B-9000 Gent, Belgium: Wim.Cosyn@UGent.be;

on which we derive the plane-wave impulse approximation and final-state interaction parts of the scattering. An overview of the various approximations used in this derivation is also given. In Sec. III, the results of our model calculations are discussed and compared to the data from the Deeps experiment performed at JLab [4]. Finally, conclusions are given in Sec. IV.

II. FORMALISM

A. General structure of the reaction

We consider the process

$$e + d \to e' + p_s + X, \tag{1}$$

in which incoming electron e has energy E_e, while $E_{e'}$ and θ_e denote the energy and scattering angle of the final electron e'. We define the laboratory frame four-momenta of the involved particles as $p_D \equiv (M_D, 0)$ for the deuteron, $q \equiv (\nu, \vec{q})$ for the virtual photon (with the z axis chosen along $\vec{q}$), $p_s \equiv (E_s = \sqrt{\vec{p}_s^2 + m_p^2}, \vec{p}_s)$ for the spectator proton, and $p_x \equiv (E_X, \vec{p}_X) = (\nu + M_D - E_s, \vec{q} - \vec{p}_s)$ the center-of-mass momentum of the undetected produced hadronic system X. We can express the differential cross section for process (1) through the four independent DIS structure functions in the following form:

$$\begin{aligned}\frac{d\sigma}{dx\,dQ^2 d\phi_{e'}\frac{d^3p_s}{2E_s(2\pi)^3}} = \frac{2\alpha_{\rm EM}^2}{xQ^4}\left(1 - y - \frac{x^2y^2m_n^2}{Q^2}\right)\Bigg[F_L^D(x, Q^2) \\ + \left(\frac{Q^2}{2|q|^2} + \tan^2\frac{\theta_e}{2}\right)\frac{\nu}{m_n}F_T^D(x, Q^2) \\ + \sqrt{\frac{Q^2}{|q|^2} + \tan^2\frac{\theta_e}{2}}\cos\phi\, F_{TL}^D(x, Q^2) \\ + \cos 2\phi\, F_{TT}^D(x, Q^2)\Bigg].\end{aligned} \tag{2}$$

Here, $\alpha_{\rm EM}$ is the fine-structure constant, $-Q^2 = \nu^2 - \vec{q}^2$ is the four-momentum transfer, Bjorken $x = \frac{Q^2}{2m_n x}$ (with m_n the mass of the neutron), $y = \frac{\nu}{E_e}$, and ϕ is the angle between the scattering (e, q) and reaction (q, p_s) planes.

We now define the nuclear electromagnetic tensor as

$$\begin{aligned}W_D^{\mu\nu} = \frac{1}{4\pi M_D}\frac{1}{3}\sum_X\sum_{s_s, s_x, s_D}\langle Ds_D|J^{\dagger\mu}|Xs_x, p_s s_s\rangle\langle Xs_x, p_s s_s| \\ \times J^\nu|Ds_D\rangle(2\pi)^4\delta^4(q + p_D - p_s - p_x)d^3\tau_x,\end{aligned} \tag{3}$$

with $d^3\tau_x$ a phase-space factor for X and s_D, s_s, and s_x the spin projection of the deuteron, spectator proton, and X, respectively. The four deuteron semi-inclusive structure functions $F_i^D(x, Q^2)$ are related to components of the nuclear electromagnetic tensor $W_D^{\mu\nu}$ as follows:

$$\begin{aligned}F_L^D(x, Q^2) &= \nu\frac{Q^4}{|q|^4}W_D^{00}(x, Q^2), \\ F_T^D(x, Q^2) &= m_n\left[W_D^{xx}(x, Q^2) + W_D^{yy}(x, Q^2)\right], \\ F_{TL}^D(x, Q^2)\cos\phi &= -2\nu\frac{Q^2}{|q|^2}W_D^{0x}(x, Q^2), \\ F_{TT}^D(x, Q^2)\cos 2\phi &= \nu\frac{Q^2}{2|q|^2}\left[W_D^{xx}(x, Q^2) - W_D^{yy}(x, Q^2)\right].\end{aligned} \tag{4}$$

B. Main approximations

In the further derivations we use the following approximations that are based largely on the general properties of DIS scattering as well as properties of the subsequent small-angle rescattering of the fast moving hadronic system off the slow recoil nucleon:

(i) Virtual nucleon approximation: To treat the electromagnetic interaction with the bound nucleon in the deuteron we use the virtual nucleon approximation (VNA) in which it is assumed that the virtual photon interacts with the off-shell nucleon in the deuteron while the second nucleon is on its mass shell [1,7,16]. The VNA is based on the following main assumptions: (a) only the pn component of the deuteron wave function is considered in the reaction, (b) the negative energy projection of the virtual nucleon propagator gives negligible contribution to the scattering amplitude, and (c) interactions of the virtual photon with exchanged mesons is neglected. Assumptions (a) and (b) can be satisfied when the momentum of the spectator proton is limited to $p_s \leqslant 700$ MeV/c [17], while (c) is satisfied at large Q^2 (>1 GeV^2) [15,18].

The electromagnetic tensor of the γN interaction is off-shell and the gauge invariance is restored by expressing the longitudinal component of the electromagnetic current through its 0th component as follows:

$$J^3 = \frac{q_0}{q_3}J^0. \tag{5}$$

The nuclear wave function in the VNA is normalized to account for the baryon number conservation [19–22]:

$$\int \alpha|\Psi_D(p)|^2 d^3p = 1, \tag{6}$$

where $\alpha = 2 - \frac{2(E_s - p_{s,z})}{M_D}$ is the light cone momentum fraction of the deuteron carried by the bound nucleon normalized in such a way that the half of the deuteron momentum fraction corresponds to $\alpha = 1$. Because of the virtuality of interacting nucleon it is impossible to satisfy the momentum sum rule at the same time. As a result

$$\int \alpha^2|\Psi_D(p)|^2 d^3p < 1, \tag{7}$$

which can be qualitatively interpreted as part of the deuteron momentum fraction being distributed to non-nucleonic degrees of freedom which are unaccounted for within the VNA.

By applying the VNA for calculation of the matrix element $\langle Xs_x, p_s s_s|J^\mu|Ds_D\rangle$, we can limit the

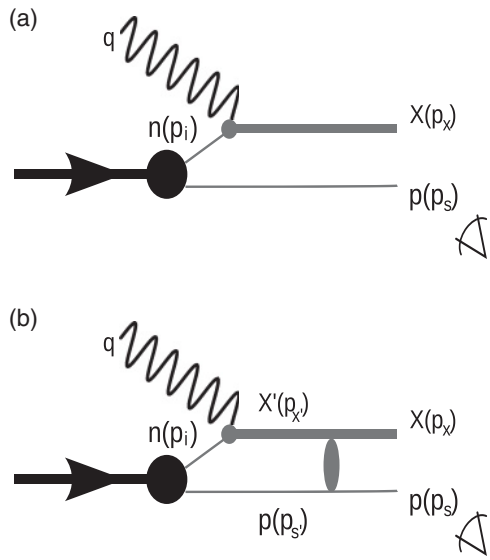

FIG. 1. Diagrams entering in the model for the ^{2}H$(e, e' p_s)X$ reaction. Panel (a) shows the plane-wave contribution. Panel (b) shows the FSI term.

Feynman diagrams taken into account to those of Fig. 1 in which Fig. 1(a) represents the plane-wave impulse approximation (PWIA) diagram. Here DIS occurs on the neutron and the proton is left in the on-shell positive energy state without further interaction in the final state. The diagram of Fig. 1(b) shows again DIS on the neutron, which is afterward followed by a $X'p \to Xp$ rescattering. In calculating this diagram we have to sum over the all possible intermediate X' states.

The calculation of the final-state interactions is based on the following main assumptions for the rescattering diagram of Fig. 1(b).

(ii) Diffractive form of the rescattering amplitude: In the considered reaction the FSI represents a small-angle rescattering of the DIS products off the slow spectator nucleon. It is in principle a very complex problem to account for the details of the interaction of the intermediate "X'" state since its structure depends on the Q^2 (x_{Bj}) and the produced mass W of the $\gamma^* N$ reaction. However, in the limit where the produced intermediate and final masses are small compared to the transferred momenta:

$$q \gg M_{X'}, M_{X'}, \tag{8}$$

one can assume that the propagation of the produced hadronic system is eikonal and the general structure of the small-angle rescattering is diffractive. The approximation of Eq. (8) allows one to model the FSI amplitude of the hadronic X' system in the following form:

$$\sum_{X'} f_{X'N,XN} = f_{XN}(t, Q^2, x_{Bj}) = \sigma_{\rm tot}(Q^2, x_{Bj})[i + \epsilon(Q^2, x_{Bj})]e^{\frac{B(Q^2, x_{Bj})}{2} t}, \tag{9}$$

where the sum of the all possible $X'N \to XN$ amplitudes are represented in the effective diffractive amplitude form, $f_{XN}(t, Q^2, x_{Bj})$ with effective total cross section $\sigma_{\rm tot}$, real part ϵ, and slope factor B. A similar approximation is used for the FSI studies in semi-inclusive DIS scattering [1,6–11] as well as for studies of color transparency phenomena in which the intermediate state represents an off-shell coherent composite system with reduced interaction cross section (see, e.g., Refs. [13,23–28]). In principle, a more elaborate model that sums the contribution of different resonances as, e.g., in Ref. [29] could be used but this would go beyond the goal in this paper of describing the reaction with the basic elements of high-energy rescattering.

(iii) Factorization: In the situation in which momentum transfer in DIS exceeds the momentum of the recoil slow nucleon one can factorize DIS scattering from the amplitude of the final-state interaction. Such an approximation commonly referred to as distorted-wave impulse approximation (DWIA) is valid in the limit of $\sqrt{Q^2} \gg p_s$, in which case the electromagnetic current is insensitive to the momentum of the stuck nucleon. The validity of the DWIA was checked quantitatively for quasielastic scattering in the case of ^{2}H$(e, e'N)N$ reactions [17,30]. These calculations demonstrated that for $Q^2 = 2$–4 GeV^2 factorization approximation works reasonably well for up to $p_s = 400$ MeV$/c$ and then at larger momenta it systematically underestimates the FSI contribution as compared to the prediction based on an unfactorized calculation. The underestimation can be understood qualitatively, since in the case of nonfactorization the amplitude of electromagnetic interaction enters in the FSI amplitude at smaller values of bound nucleon momenta and therefore predicts more rescattering than the DWIA does. This pattern one also expects to be generally valid for inelastic interactions.

(iv) Approximate conservation law of high-energy small-angle scatterings: In the eikonal regime of small-angle scattering there is an approximate conservation law for the "$-$" component[1] of slow nucleon momenta involved in the scattering [15]. According to this law, because the fast particle attains its momentum after the small-angle scattering the slow nucleon will conserve its "$-$" component. This follows from the conservation of the "$-$" component of the total momentum in $X'N' \to XN$ scattering and relations $p_{X'-} \approx \frac{m^2_{X'} + p^2_{X'\perp}}{2q} \ll 1$ and $p_{X^-} \approx \frac{m^2_X + p^2_{X\perp}}{2q} \ll 1$ provided that the condition of Eq. (8) is satisfied. This yields:

$$p_{s'-} - p_{s-} = p_{X^-} - p_{X'-} \approx 0. \tag{10}$$

Using this relation and assuming that

$$p^2_{s\perp} < k^2_\perp, \tag{11}$$

[1]The $\pm$ components of the momentum is defined as $p_\pm = E \pm p_z$.

where $k_\perp^2$ is the average transferred momentum in the rescattering one obtains:

$$\begin{aligned} m_X^2 &= (p_{X'} + p_{s'} - p_s)^2 \\ &\approx m_{X'}^2 - 2p_{X'\perp}(p_{s'\perp} - p_{s\perp}) - k_\perp^2 \\ &\approx m_{X'}^2 + k_\perp^2 > m_{X'}^2, \end{aligned} \tag{12}$$

where in the above derivation we used the fact that in the limit of Eq. (11) $p_{X'\perp} = -p_{s'\perp} \approx k_\perp$. The above result qualitatively means that in the situation in which two collinear particles are produced by the diffractive scattering of a fast and slow particle with equal and opposite transverse momenta the mass of the final fast particle is larger than the initial mass.

Using the characteristic values of the diffractive slope, $B = 4 - 6$ GeV^{-2}, one can estimate $k_{\perp,\mathrm{RMS}} \approx$ 500–600 MeV/c. This estimate of $k_\perp$ and Eq. (11) further constrains the values of spectator nucleon momenta for which the calculations will be valid.

Our derivations in the following two subsections are based on the above assumptions.

C. Plane-wave impulse approximation

Applying Feynman diagram rules (see, e.g., Ref. [15]) and introducing the effective wave functions of the final hadronic system X, the amplitude of the PWIA diagram in Fig. 1(a) takes the following form:

$$\begin{aligned} &\langle X s_x, p_s s_s | J^\mu | D s_D \rangle^{\mathrm{PWIA}} \\ &\quad = -\bar{\Psi}_X(p_X, s_X)\Gamma^\mu_{\gamma^* X} \frac{\not{p}_i + m_n}{p_i^2 - m_n^2} \bar{u}(p_s, s_s)\Gamma_{DNN}\chi^{s_D}. \end{aligned} \tag{13}$$

Here, Ψ_X is a wave function for X and $\Gamma^\mu_{\gamma^* X}$ represents the electromagnetic vertex of the DIS. The transition of the deuteron into a pn system is described by the vertex function Γ_{DNN} and χ^{s_D} denotes the spin-wave function of the deuteron. The laboratory frame four-momentum of the struck neutron p_i in the PWIA is defined as

$$p_i = (M_D - E_s, -\vec{p}_s). \tag{14}$$

We now split the initial nucleon propagator in on-shell and off-shell parts by adding and subtracting an on-shell energy part:

$$\not{p}_i + m_n = \not{p}_i^{\mathrm{on}} + m_n + \left(E_i^{\mathrm{off}} - E_i^{\mathrm{on}}\right)\gamma^0, \tag{15}$$

with $E_i^{\mathrm{off}} = M_D - E_s$ and $E_i^{\mathrm{on}} = \sqrt{m_n^2 + p_s^2}$. We then write

$$\not{p}_i^{\mathrm{on}} + m_n = \textstyle\sum_{s_i} u(p_i, s_i)\bar{u}(p_i, s_i), \tag{16}$$

$$\left(E_i^{\mathrm{off}} - E_i^{\mathrm{on}}\right)\gamma^0 \approx \tfrac{E_i^{\mathrm{off}} - E_i^{\mathrm{on}}}{2m_n}\gamma^0 \textstyle\sum_{s_i} u(p_i, s_i)\bar{u}(p_i, s_i), \tag{17}$$

where in the last equation we used $\sum_{s_i} u(p_i, s_i)\bar{u}(p_i, s_i) \approx 2m_n I$, which is consistent with neglecting the negative energy component of the bound nucleon propagator. Now, with the definition [31,32]

$$\Psi_D^{s_D}(p_1 s_1, p_2 s_2) = -\frac{\bar{u}(p_1, s_1)\bar{u}(p_2, s_2)\Gamma_{DNN}\chi^{s_D}}{\left(p_1^2 - m_1^2\right)\sqrt{2}\sqrt{2(2\pi)^3\left(p_2^2 + m_2^2\right)^{\frac{1}{2}}}}, \tag{18}$$

we can write Eq. (13) as

$$\begin{aligned} &\langle X s_x, p_s s_s | J^\mu | D s_D \rangle^{\mathrm{PWIA}} \\ &\quad = \sqrt{2}\sqrt{(2\pi)^3 2E_s}\sum_{s_i}\langle X s_x | \Gamma^\mu_{\gamma^* N,X} \\ &\qquad \times |p_i s_i\rangle \left(1 + \frac{E_i^{\mathrm{off}} - E_i^{\mathrm{on}}}{2m_n}\gamma^0\right)\Psi_D^{s_D}(p_i s_i, p_s s_s). \end{aligned} \tag{19}$$

Even though Eq. (13) is gauge invariant, one cannot calculate the off-shell part of the current explicitly since the form of the electromagnetic vertex $\Gamma^\mu_{\gamma^* N,X}$ is unknown. Instead, in the reminder of the derivation the term $\frac{E_i^{\mathrm{off}} - E_i^{\mathrm{on}}}{2m_n}\gamma_0$ associated with the off-shell behavior of the photon-neutron interaction will be dropped and the gauge invariance will be restored through Eq. (5). Inserting Eq. (19) in Eq. (3) we obtain for the PWIA contribution

$$\begin{aligned} W_D^{\mu\nu} = \frac{1}{4\pi M_D}\frac{2}{3}\sum_X \sum_{s_s, s_x, s_D, s_i, s_i'} &\left\langle p_i s_i \middle| \Gamma^{\dagger\mu}_{\gamma^* N,X} \middle| X s_x \right\rangle \langle X s_x | \\ &\times \Gamma^\nu_{\gamma^* N,X} | p_i s_i' \rangle (2\pi)^4 \delta^4(q + p_i - p_x) d^3\tau_x (2\pi)^3 2E_s \\ &\times \Psi^{\dagger s_D}(p_i s_i, p_s m_s)\Psi^{s_D}(p_i s_i', p_s m_s). \end{aligned} \tag{20}$$

We can simplify this further by using

$$\begin{aligned} \sum_{s_D, s_s} \Psi^{\dagger s_D}(p_i s_i, p_s m_s)\Psi^{s_D}(p_i s_i', p_s m_s) \\ = \sum_{s_D, s_s} |\Psi^{s_D}(p_i s_i, p_s s_s)|^2 \delta_{s_i, s_i'} \end{aligned} \tag{21}$$

and

$$\begin{aligned} \sum_{s_D, s_s} |\Psi^{s_D}(p_i s_i = +1, p_s s_s)|^2 \\ = \sum_{s_D, s_s} |\Psi^{s_D}(p_i s_i = -1, p_s s_s)|^2. \end{aligned} \tag{22}$$

Equation (20) then becomes

$$\begin{aligned} W_D^{\mu\nu} = \frac{1}{4\pi M_D}\sum_X \sum_{s_x, s_i} &\left\langle p_i s_i \middle| \Gamma^{\dagger\mu}_{\gamma^* N,X} \middle| X s_x \right\rangle \left\langle X s_x \middle| \Gamma^\nu_{\gamma^* N,X} \middle| p_i s_i \right\rangle \\ &\times (2\pi)^4 \delta^4(q + p_i - p_x) d^3\tau_x (2\pi)^3 2E_s \\ &\times \frac{1}{3}\sum_{s_D, s_s, s_i'} |\Psi^{s_D}(p_i s_i', p_s s_s)|^2. \end{aligned} \tag{23}$$

After defining the spectral function

$$S(p_s) \equiv \frac{1}{3}\sum_{s_D, s_s, s_i} |\ \Psi^{s_D}(p_i s_i, p_s s_s)\ |^2, \tag{24}$$

and using the following expression for the nuclear tensor of the DIS process on a moving nucleon

$$W_N^{\mu\nu} = \frac{1}{4\pi m_n}\frac{1}{2}\sum_X \sum_{s_x,s_i} \langle p_i s_i | \Gamma^{\dagger\mu}_{\gamma^* N,X} | X s_x\rangle \langle X s_x | \Gamma^{\nu}_{\gamma^* N,X} | p_i s_i\rangle \times (2\pi)^4 \delta^4(q + p_i - p_x) d^3\tau_X, \quad (25)$$

we can write Eq. (23) as

$$W_D^{\mu\nu} = W_N^{\mu\nu} S(p_s)(2\pi)^3 2E_s, \quad (26)$$

where we also used $\frac{2m_n}{M_D} \approx 1$. Substituting Eq. (26) in (4) allows us to relate the four deuteron DIS structure functions to the nucleon structure functions. After straightforward calculations one obtains the following relations for the deuteron structure functions:

$$F_L^D(x, Q^2) = \left\{ \left[\alpha_i + \frac{\alpha_q (p_i \cdot q)}{Q^2} \right]^2 (1 + \cos\delta)^2 \frac{\nu}{\hat{\nu}} F_{2N} \times (\alpha_i, \hat{x}, Q^2) - \frac{\nu}{m_n} \sin^2\delta F_{1N}(\alpha_i, \hat{x}, Q^2) \right\} \times S(p_s)(2\pi)^3 2E_s, \quad (27)$$

$$F_T^D(x, Q^2) = \left\{ 2F_{1N}(\alpha_i, \hat{x}, Q^2) + \frac{p_T^2}{m_n \hat{\nu}} F_{2N}(\alpha_i, \hat{x}, Q^2) \right\} \times S(p_s)(2\pi)^3 2E_s, \quad (28)$$

$$F_{TT}^D(x, Q^2) = \frac{\nu}{\hat{\nu}} \frac{p_T^2}{m_n^2} \frac{\sin^2\delta}{2} F_{2N}(\alpha_i, \hat{x}, Q^2) S(p_s)(2\pi)^3 2E_s, \quad (29)$$

$$F_{TL}^D(x, Q^2) = 2(1 + \cos\delta)\frac{p_T}{m_n}\left[\alpha_i + \frac{\alpha_q (p_i \cdot q)}{Q^2} \right]\frac{\nu}{\hat{\nu}} \times F_{2N}(\alpha_i, \hat{x}, Q^2) S(p_s)(2\pi)^3 2E_s, \quad (30)$$

where $\alpha_i = \frac{2p_i^-}{M_D}$, $\alpha_q = \frac{2q^-}{M_D}$, $\hat{\nu} = \frac{p_i \cdot q}{m_n}$, $\hat{x} = \frac{Q^2}{2m_n\hat{\nu}}$,$\cos\delta = \frac{\nu}{|q|}$, $\sin^2\delta = \frac{Q^2}{|q|^2}$, and F_{1N}, F_{2N} are the effective nucleon structure functions, which are defined at $\hat{x}$ and in principle could be modified due to the nuclear binding (see, e.g., Ref. [1]).

Note that the inclusive F_2, F_1, and F_L^{in} structure functions of the deuteron can be obtained from the above given semi-inclusive structure functions through the following relations:

$$F_{2,D} = \sum_N \int \left(F_L^D + \frac{Q^2}{2|q|^2}\frac{\nu}{m_N} F_T^D \right) \frac{d^3 p_s}{(2\pi)^2 2E_s} \approx \sum_N \int \left(F_L^D + x F_T^D \right) \frac{d^3 p_s}{(2\pi)^2 2E_s},$$

$$F_{1,D} = \sum_N \int \frac{F_T^D}{2} \frac{d^3 p_s}{(2\pi)^2 2E_s},$$

$$F_{L,D}^{in} \equiv F_{2,D} - 2x F_{1,D} = \sum_N \int \left[F_L^D + \left(\frac{Q^2}{2|q|^2}\frac{\nu}{m_N} - x \right) F_T^D \right] \frac{d^3 p_s}{(2\pi)^2 2E_s} \approx \sum_N \int F_L^D \frac{d^3 p_s}{(2\pi)^2 2E_s}, \quad (31)$$

where one sums by the contributions of both the proton and neutron. The right-hand side parts of the equations represent the expressions in the case of the Bjorken limit with x fixed and $Q^2, \nu \to \infty$.

D. Final-state interaction amplitude

With the same notations as in Sec. II C, we can write for the amplitude of the FSI diagram in Fig. 1(b)

$$\langle X s_x, p_s s_s | J^\mu | D s_D \rangle^{\rm FSI} = -\sum_{X'} \int \frac{d^4 p_{s'}}{i(2\pi)^4} \frac{\bar{\Psi}_X(p_X, s_X)\bar{u}(p_s, s_s) F_{X'N,XN}[\not{p}_{s'} + m_p]}{\left[p_{s'}^2 - m_p^2 + i\epsilon\right]} \times \frac{G(P_{X'})\Gamma^\mu_{\gamma^* X'}[\not{p}_{i'} + m_n]\Gamma_{DNN}\chi^{s_D}}{\left[p_{X'}^2 - m_{X'}^2 + i\epsilon\right]\left[p_{i'}^2 - m_n^2 + i\epsilon\right]}, \quad (32)$$

where $G(p_{X'})$ describes the Green's function of the intermediate state X' that has four-vector $p_{X'} \equiv p_{i'} + q = (\nu + M_D - E_{s'}, \vec{q} - \vec{p}_{s'})$ and a mass $m_{X'}$, while the intermediate struck neutron has four-vector $p_{i'} = (M_D - E_{s'}, -\vec{p}_{s'})$. $F_{X'N,XN}$ represents the invariant $X'N \to XN$ scattering amplitude which is expressed in the following form

$$F_{X'N,XN}(s,t) = \sqrt{(s - (m_n - m_{X'})^2)(s - (m_n + m_{X'})^2)} \times f_{X'N,XN}(s,t) = \beta(s, m_{X'}) f_{X'N,XN}(s,t), \quad (33)$$

with $s = (p_X + p_s)^2 = (p_{X'} + p_{s'})^2$ the total invariant energy of the scattering system and the scattering amplitude $f_{X'N,XN}$ defined such that $\mathrm{Im}[f_{X'N,XN}(t \equiv 0)] = \sigma_{\rm tot}$, where $\sigma_{\rm tot}$ represents the total cross section of the scattering of the produced X' system off the spectator nucleon. Based on the assumptions of the VNA from Sec. II B, the intermediate spectator nucleon can be placed on the nucleon mass-shell by integrating $d^0 p_{s'}$ through the positive energy pole only:

$$\int \frac{d^0 p_{s'}}{p_{s'}^2 - m_p^2 + i\epsilon} \to -i\frac{\pi}{E_{s'}}. \quad (34)$$

This allows us to use the on-shell spinor relation $\not{p}_{s'} + m_p = \sum_{s_{s'}} u(p_{s'}, s_{s'})\bar{u}(p_{s'}, s_{s'})$ in the nominator of Eq. (32). For the propagator of the initial neutron we again use the prescription of Eqs. (15) to (16). For the intermediate state X' an on-shell relation for the Green's function $G(p_{X'}) = \sum_{s_{x'}} \psi(p_{x'}, s_{x'})\psi^\dagger(p_{x'}, s_{x'})$ is used as in the high Q^2 limit the off-shell contribution in Eq. (32) becomes small due to the large momentum involved in the propagator of the intermediate state X'. By making use of $p_X^2 = (q + p_D - p_s)^2 = m_X^2$, the denominator of the X' propagator can be rewritten as

$$p_{X'}^2 - m_{X'}^2 + i\epsilon = 2\,|\,\vec{q}\,|\,(p_{s',z} - p_{s,z} + \Delta + i\epsilon), \quad (35)$$

with

$$\Delta = \frac{\nu + M_D}{|\,\vec{q}\,|}(E_s - E_{s'}) + \frac{m_X^2 - m_{X'}^2}{2\,|\,\vec{q}\,|}. \quad (36)$$

All this combined with the deuteron wave function of Eq. (18) allows us to write the FSI amplitude as

$$\begin{aligned}&\langle Xs_x,\, p_s s_s|J^\mu|Ds_D\rangle^{\rm FSI}\\&=-\sum_{X'}\sum_{s_i,s_{s'},s_{x'}}\int\frac{d^3p_{s'}}{(2\pi)^3}\beta(s,m_{X'})\langle Xs_x,\, p_s s_s|f_{X'N,XN}(s,t)\\&\quad\times|X's_{x'},\, p_{s'}s_{s'}\rangle\frac{\langle X's_{x'}|\Gamma^\mu_{\gamma^*N,X'}|p_{i'}s_i\rangle\Psi^{s_D}(p_{i'}s_i,\, p_{s'}s_{s'})}{4E_{s'}\mid\vec q\mid[p_{s',z}-p_{s,z}+\Delta+i\epsilon]}\\&\quad\times\sqrt{2}\sqrt{(2\pi)^3 2E_{s'}}.\end{aligned}\tag{37}$$

In a next step, we assume the rescattering amplitude conserves the helicities of all particles involved

$$\begin{aligned}&\langle Xs_x,\, p_s s_s|f_{X'N,XN}(s,t)|X's_{x'},\, p_{s'}s_{s'}\rangle\\&\quad\approx\langle Xs_x,\, p_s s_s|f_{X'N,XN}(s,t)|X's_x,\, p_{s'}s_s\rangle\delta_{s_s,s_{s'}}\delta_{s_x,s_{x'}},\end{aligned}\tag{38}$$

and we use the following approximation to take the current matrix element out of the integration:

$$\left\langle X's_x\middle|\Gamma^\mu_{\gamma^*N,X'}\middle|p_{i'}s_i\right\rangle\approx\left\langle Xs_x\middle|\Gamma^\mu_{\gamma^*N,X}\middle|p_i s_i\right\rangle.\tag{39}$$

This allows us to factorize the nuclear tensor again like in Eq. (26). For the sum of the plane-wave and FSI amplitudes, we then obtain

$$W_D^{\mu\nu}=W_N^{\mu\nu}S^{\rm dist.}(p_s)(2\pi)^3 2E_s,\tag{40}$$

with the distorted spectral function defined as

$$\begin{aligned}&S(p_s)^{\rm dist.}\\&\equiv\frac{1}{3}\sum_{s_D,s_s,s_i}\left|\Psi^{s_D}(p_i s_i,\, p_s s_s)-\sum_{X'}\int\frac{d^3p_{s'}}{(2\pi)^3}\frac{\beta(s,m_{X'})}{4\mid\vec q\mid\sqrt{E_s E_{s'}}}\right.\\&\quad\times\langle Xs_x,\, p_s s_s|f_{X'N,XN}(s,t)|X's_x,\, p_{s'}s_s\rangle\\&\quad\left.\times\frac{\Psi^{s_D}(p_{i'}s_i,\, p_{s'}s_s)}{[p_{s',z}-p_{s,z}+\Delta+i\epsilon]}\right|^2.\end{aligned}\tag{41}$$

E. Distorted spectral function

For calculation of the distorted spectral function in Eq. (41) we use VNA model of deuteron wave function of Eq. (18) which can be related to the nonrelativistic deuteron wave function by [7,17,20]

$$\Psi_D(p)=\Psi_D^{\rm NR}(p)\sqrt{\frac{M_D}{2(M_D-E_s)}},\tag{42}$$

which explicitly conserves the baryonic sum rule of Eq. (6). The parametrizations for the nonrelativistic wave function used in this paper all take the following form (see, e.g., Refs. [33,34]):

$$\begin{aligned}&\Psi_D^{s_D}(\vec p s_1,-\vec p s_2)\\&\quad=\chi^{\dagger,s_1}\chi^{\dagger,s_2}\left[\sum_j\frac{c_j}{p^2+m_j^2}+\sum_j\frac{d_j}{p^2+m_j^2}\mathcal{S}(\vec p)\right]\chi^{s_D},\end{aligned}\tag{43}$$

with $\mathcal{S}(\vec p)=\sqrt{\frac{1}{8}}(\frac{3\vec\sigma_1\cdot\vec p\vec\sigma_2\cdot\vec p}{p^2}-\vec\sigma_1\cdot\vec\sigma_2)$ the tensor operator. Such form allows us to perform the $dp_{s',z}$ integration in the distorted spectral function of Eq. (41) analytically by making use of the pole structure of these parametrizations as well as the pole of the propagator in Eq. (41) at $\tilde p_{s',z}=p_{s,z}-\Delta$. In the latter case the mass of the produced intermediate state $m_{X'}$ enters in the phase factor Δ. We note that even though we sum over the all possible intermediate states X' the mass $m_{X'}$ is defined by the four-momenta of the interacting virtual nucleon and virtual photon q. Based on the assumption that FSI is dominated by a small-angle diffractive scattering, the phase factor Δ is evaluated based on the property of the approximate conservation law of "$-$" components of rescattering particle momenta discussed in Sec. II B. Taking into account the relation of Eq. (12) in the definition of the Δ factor in Eq. (36) we evaluate:

$$\begin{aligned}\Delta&=\frac{\nu+M_D}{\mid\vec q\mid}(E_s-m_p)+\frac{m_X^2-\gamma}{2\mid\vec q\mid}\quad\text{for}\,\gamma\leqslant m_X^2,\\\Delta&=\frac{\nu+M_D}{\mid\vec q\mid}(E_s-m_p)\quad\text{for}\,\gamma>m_X^2,\end{aligned}\tag{44}$$

where $\gamma\equiv m_{X'}^2(p_{i'}=0)=m_n^2+2m_n\nu-Q^2$ is the produced DIS mass off the stationary nucleon. The latter approximation for $m_{X'}$ is justified by the fact that due to the peaking of the deuteron wave function at small momenta the integrand in Eq. (41) is dominated by smaller virtual nucleon momenta than in the PWIA term.

The $p_{s',z}$ integration in Eq. (41) is performed analytically by closing the integration contour into either the upper or lower complex hemispheres. In both cases[2] one obtains:

$$\begin{aligned}\int dp_{s',z}\frac{\Psi^{s_D}(p_{i'}s_i,\, p_{s'}s_s)}{p_{s',z}-p_{s,z}+\Delta+i\epsilon}&=-i\pi\,\Psi^{s_D}(\tilde p_{s,z},\, p_{s',\perp},\, s_i,\, s_s)\\&\quad-\pi\,\tilde p_{s,z}\tilde\Psi(\tilde p_{s,z},\, p_{s',\perp},\, s_i,\, s_s),\end{aligned}\tag{45}$$

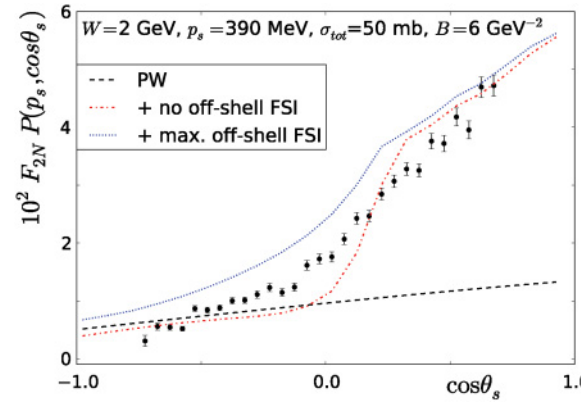

FIG. 2. (Color online) Comparison between the Deeps data [4] and model calculations at $Q^2=1.8$ GeV^2. The dashed black curve is a plane-wave calculation, the others include final-state interactions. The effective total cross section and slope parameter in the final-state interaction amplitude are fixed to $\sigma_{\rm tot}=50$ mb, $B=6$ GeV^{-2}, and $\epsilon=-0.5$. The dotted blue curve has an off-shell rescattering amplitude amplitude equal to the on-shell one (maximal off-shell FSI); the dash-dotted red curve has no off-shell FSI.

[2]See Appendix B of Ref. [15] for details of integration.

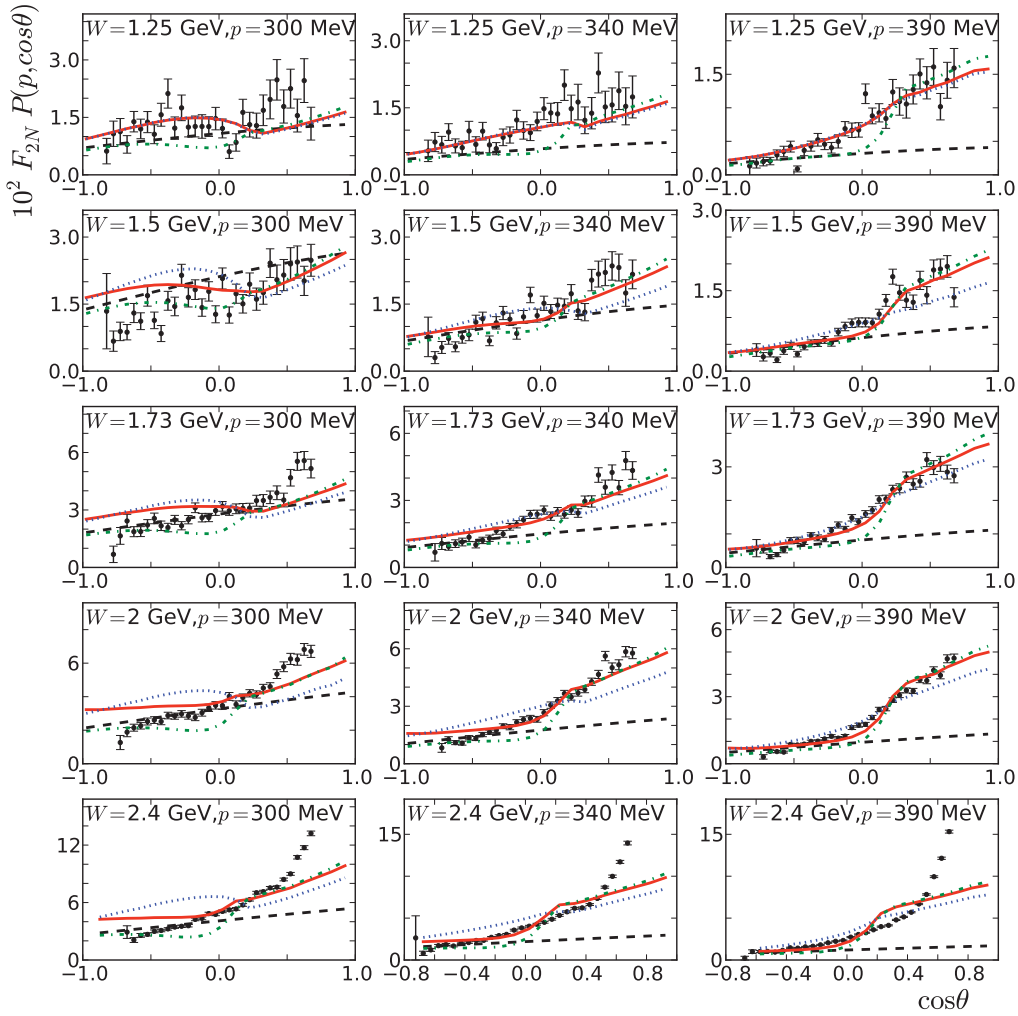

FIG. 3. (Color online) Comparison between the Deeps data [4] and model calculations at $Q^2 = 1.8$ GeV^2 at measured values of invariant mass W and spectator momenta p ($\equiv p_s$ in the text) of 300, 340, and 390 MeV. The dashed black curve is a plane-wave calculation, and the others includes final-state interactions. The effective total cross section and slope parameter in the final-state interaction amplitude are fitted parameters for each W, the real part is fixed at $\epsilon = -0.5$. The dot-dashed green curve only considers on-shell rescattering, the dotted blue curve has an off-shell rescattering amplitude equal to the on-shell one and the full red curve uses the off-shell parameterization of Eq. (55).

where the distorted-wave function $\tilde{\Psi}$ is defined in Eq. (47). In the above equation the first term can be identified with the (imaginary) on-shell part of the $p_{s',z}$ propagator while the second term with the (real) principal value integration. Inserting Eq. (45) into Eq. (41) one obtains for the distorted spectral function:

$$S(p_s)^{\text{dist.}} = \frac{1}{3}\sum_{s_D,s_s,s_i}\Bigg|\Psi^{s_D}(\vec{p}_s,s_i,s_s) + \frac{i}{2}\sum_{X'}\int\frac{d^2p_{s',\perp}}{(2\pi)^2} \times \frac{\beta(s,m_{X'})}{4\mid\vec{q}\mid\sqrt{E_sE_{s'}}}\left[\left\langle X,\,p_s\middle|f^{\text{on}}_{X'N,XN}(s,t)\middle|X',\,\tilde{p}_{s'}\right\rangle \Psi^{s_D}(\tilde{p}_{s'},s_i,s_s) - i\langle X,\,p_s|f^{\text{off}}_{X'N,XN}(s,t) \times|X',\,\tilde{p}_{s'}\rangle\tilde{p}_{s',z}\tilde{\Psi}^{s_D}(\tilde{p}_{s'},s_i,s_s)\right]\Bigg|^2, \tag{46}$$

where for the distorted-wave function of the deuteron one obtains:

$$\tilde{\Psi}^{s_D}(p_s,s_1,s_2) = \left\{u_1(p_s) + \frac{w_1(p_s)}{\sqrt{8}}\mathcal{S}(p_s) + \frac{w_2(p_s)}{\sqrt{8}}\frac{p^2_{s,\perp}}{p^2_{s,z}} \times[\mathcal{S}(p_s) - \mathcal{S}(p_{s,\perp})]\right\}\chi^{s_1}\chi^{s_2}, \tag{47}$$

with

$$u_1(p) = \sum_j \frac{c_j}{\sqrt{p^2_\perp + m_j^2}p^2 + m_j^2},$$
$$w_1(p) = \sum_j \frac{d_j}{\sqrt{p^2_\perp + m_j^2}p^2 + m_j^2}, \tag{48}$$
$$w_2(p) = \sum_j \frac{d_j}{m_j^2\sqrt{p^2_\perp + m_j^2}}.$$

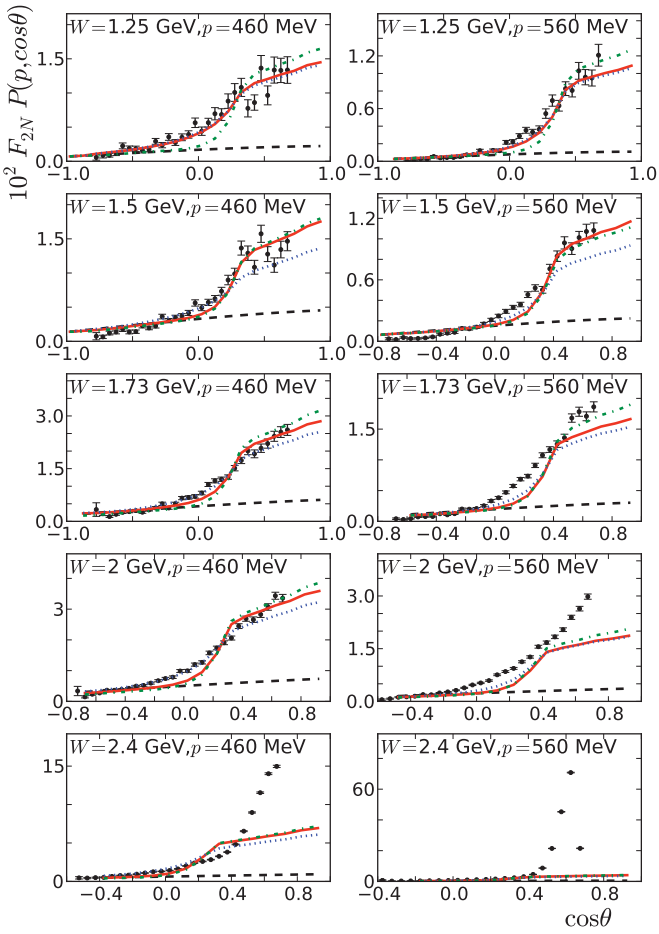

FIG. 4. (Color online) Comparison between the Deeps data [4] and model calculations at $Q^2 = 1.8$ GeV^2 at measured values of invariant mass W and spectator momenta p ($\equiv p_s$ in the text) of 460 and 560 MeV. Graphs as in Fig. 3.

The distorted spectral function in Eq. (46) depends on the intermediate state X' through the final-state rescattering amplitude only. As a result, one can factorize the sum over the X' in the form of Eq. (9) and represent the on-shell forward-scattering amplitude in the form of

$$f_{XN}^{\rm on} = \sigma_{\rm tot}(Q^2, W)[i + \epsilon(Q^2, W)]e^{\frac{B(Q^2,W)}{2}t}, \qquad (49)$$

with W the invariant mass of the produced hadronic state X. For the off-shell amplitude $f^{\rm off}$ there is no clear prescription, but following our main goal of studying the semi-inclusive DIS based only on basic properties of the high-energy scattering we identify two extreme cases for off-shell part of the rescattering amplitude, one when it is taken to be zero (no off-shell FSI) and the other in which off-shell amplitude is assumed to be equal to the on-shell amplitude $f_{XN}^{\rm on}$ referred as maximal off-shell FSI. The numerical estimates for $f_{XN}^{\rm off}$ we used in our calculations will be discussed below in Sec. III.

With this, we have all the ingredients needed to compute the cross section of Eq. (2).

III. RESULTS

A. Experimental observables

In this section, we compare calculations in our model with the first results extracted from data taken in the Deeps experiment at JLab [4]. Events of the data set were binned in Q^2, p_s, $\cos\theta_s$ (with $\theta_s = \widehat{q, p_s}$), and $\hat{x}$ (or the invariant mass of the produced hadronic state W). In order to compare our model calculations with the data, we integrate Eq. (2) over $\phi_{e'}$, use

$$\frac{d\hat{x}}{dx} = \frac{2\hat{x}^2}{x}\frac{\nu}{|q|}\left|\frac{\alpha_i}{\alpha_q} + \frac{1}{2\hat{x}}\right| \qquad (50)$$

and relate $F_{1N}(\alpha_i, \hat{x}, Q^2)$ to $F_{2N}(\alpha_i, \hat{x}, Q^2)$ for a moving nucleon:

$$F_{1N}(\alpha_i, \hat{x}, Q^2) = \frac{2\hat{x}}{1+R}\left[\left(\frac{\alpha_i}{\alpha_q} + \frac{1}{2\hat{x}}\right)^2 - \frac{p_T^2}{2Q^2}R\right] \times F_{2N}(\alpha_i, \hat{x}, Q^2), \qquad (51)$$

where $R = \frac{\sigma_L}{\sigma_T} \approx 0.18$ is the ratio of the longitudinal to transverse cross sections for scattering off the nucleon. This yields for the differential cross section:

$$\frac{d\sigma}{d\hat{x}dQ^2d^3p_s} = \frac{4\pi\alpha_{\rm EM}}{Q^2\hat{x}}\frac{|q|}{m_n}\left(1 - y - \frac{x^2y^2m_n^2}{Q^2}\right) \times \left(\frac{Q^2}{|q|^2} + \frac{2\tan^2\frac{\theta_e}{2}}{1+R}\right)\left|\frac{\alpha_i}{\alpha_q} + \frac{1}{2\hat{x}}\right|^{-1} \times \left[\left(\frac{\alpha_i}{\alpha_q} + \frac{1}{2\hat{x}}\right)^2 + \frac{p_T^2}{2Q^2}\right] \times F_{2N}(\alpha_i, \hat{x}, Q^2)S(p_s). \qquad (52)$$

Now using Eq. (52) we need to reproduce the quantity $F_{2N}P(\vec{p}_s)$ (with $P(\vec{p}_s) = \frac{\alpha_i M_D}{2(M_D - E_S)}|\Psi_D^{\rm NR}(p_s)|^2$) for which the experimental data are given in Ref. [4]. For this we divide the cross section of Eq. (52) with the following prefactor

$$\mathcal{F} = \frac{4\pi\alpha_{\rm EM}}{Q^2\hat{x}}\left[\frac{\hat{y}}{2(1+R)} + (1-\hat{y}) + \frac{p_i^2\hat{x}^2\hat{y}^2}{Q^2}\frac{1-R}{1+R}\right], \qquad (53)$$

where $\hat{y} = \frac{p_i\cdot q}{p_i\cdot k_e}$. This results to the following representations of our model calculations:

$$(F_{2N}P)_{\rm model} = \frac{1}{\mathcal{F}}\left(\frac{d\sigma}{d\hat{x}dQ^2d^3p_s}\right)_{\rm model}. \qquad (54)$$

In numerical estimates we use the SLAC parametrizations for the neutron structure functions F_{1N} and F_{2N} [35] in the calculations as these were used in the analysis of the Deeps data [4]. The arguments of the nucleon structure functions are defined from the off-shell kinematics $(p_i + q) = W^2$, where the four-momentum of the initial nucleon is defined as $p_i = p_D - p_s$. No additional modifications due to nuclear modifications like the EMC effect are assumed for the nucleon structure functions. This is in accordance to our approach of estimating the properties of the reaction based on the basic properties of the high-energy scattering rather than modeling

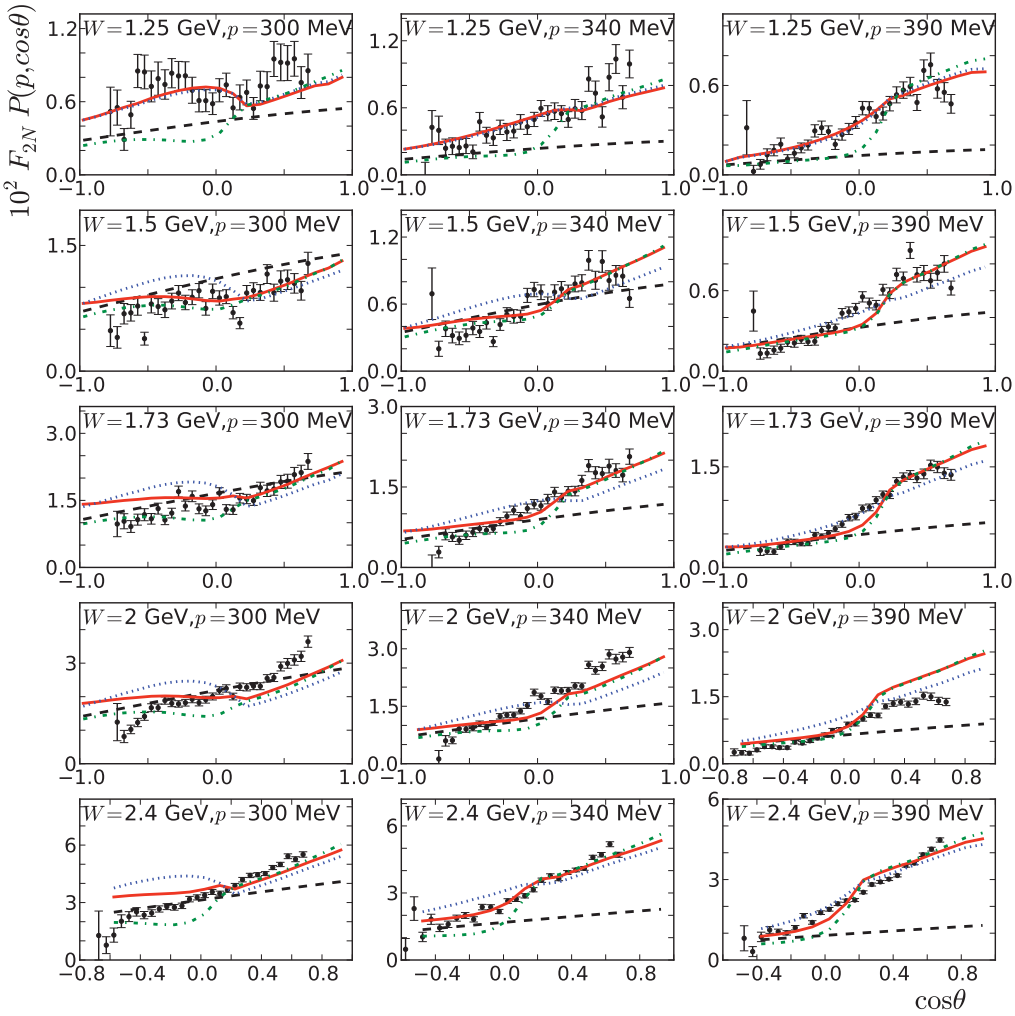

FIG. 5. (Color online) Comparison between the Deeps data [4] and model calculations at $Q^2 = 2.8$ GeV^2 at measured values of invariant mass W and spectator momenta p ($\equiv p_s$ in the text) of 300, 340, and 390 MeV. Graphs as in Fig. 3.

the specific details of the reaction. Additionally, we deem the influence of these modifications small in comparison with the typical magnitude of the experimental uncertainties to extract unambiguous information here.

B. Numerical estimates

We start first with the calculation of the quantity of Eq. (54) for the typical kinematic setting of the experiment [4] with $Q^2 = 1.8$ GeV^2, $W^2 = 2$ GeV, and $p_s = 390$ MeV/c. For on-shell part of the rescattering $XN \to XN$ amplitude we use the diffractive form of the parametrization of Eq. (9) with characteristic values of $\sigma_{\rm tot} = 50$ mb, $B = 6$ GeV^{-2}, and $\epsilon = -0.5$. Our estimate of the total XN cross section is based on the assumption that the final state consists of the hadronic state equivalent to one nucleon and one pion. In principle it is possible to develop specific model (see, e.g., Ref. [12]) describing the XN rescattering; however, we follow here our main goal of understanding how far we can go with describing data on basic properties of high-energy scattering. For the off-shell part of the XN rescattering we use two limiting cases as discussed above: $f_{XN}^{\rm off-shell} = 0$ (no off-shell FSI) and $f_{XN}^{\rm off-shell} = f_{XN}^{\rm on-shell}$ (maximal off-shell FSI). The results of these calculations are given in Fig. 2.

As the figure shows, FSI effects continuously grow in the forward angles of production of recoil proton. This result differs strikingly from the case of the quasielastic $d(e, e'N)X$ scattering in which case the FSI is maximal at transverse angles ($\sim$70°) of recoil nucleon production (see, e.g., Ref. [17]) and diminishes in the forward direction. The continuously growing FSI contribution in the forward direction for DIS scattering follows from the specific structure of the phase factors (Δ) entering in Eq. (44) which follows from Eq. (12). For forward angles the dominant mass contribution m'_X decreases, as can be seen in the stationary approximation (virtual photon energy ν decreases with forward angles). As m'_X decreases the off-diagonal mass term in Eq. (44) grows bigger and so does Δ causing the peak to shift to more forward angles.

Another observation from Fig. 2 is the relatively small contribution due to the off-shell part of the XN rescattering amplitude. This result is in agreement of the space-time

analysis of high-energy small-angle rescattering of Ref. [36], according to which the longitudinal distances that off-shell particle propagates before rescattering significantly shrinks in the high Q^2 and fixed Bjorken x limit. This results in the suppression of the off-shell part of the FSI.

The next question we address is whether the parameters of $X'N$ rescattering amplitude are sensitive to the produced DIS mass W and Q^2. For this we assume some of the parameters entering the rescattering amplitude of Eq. (9) to be free parameters. We made fits using one (effective total cross section $\sigma_{\rm tot}$) or two ($\sigma_{\rm tot}$ and slope factor B) free parameters. The real to imaginary part ratio of the amplitude was fixed at $\epsilon = -0.5$, a value extrapolated from nucleon-nucleon scattering parameterizations.

For the off-shell rescattering amplitude in addition to the above-mentioned no off-shell FSI and maximal off-shell FSI options, we consider the third approach, in which case we parameterize the off-shell amplitude as

$$f_{XN}^{\rm off} = \sigma_{\rm tot}^{\rm on}(Q^2, W_N)[i + \epsilon^{\rm on}(Q^2, W_N)]e^{-\frac{B^{\rm off}(Q^2,W_N)}{2}t}, \qquad (55)$$

where the effective cross section and real part parameters were taken equal to the on-shell ones, but the slope parameter was taken as a new free parameter in the fit. This will give us some measure of the size of the suppression as compared to the on-shell amplitude, this approach is referred to as fitted off-shell FSI.

The parameters were fitted for each (Q^2, W) to all measured spectator momenta. When comparing the results of the fits to the data it became clear that the model fits systematically underestimate the data at the highest measured spectator momentum $p_s = 560$ MeV. This may be a consequence of the factorization used in this model, which begins to break down at these momenta (see discussion in Sec. II B). In subsequent fits we decided to exclude the highest spectator momentum as we deem the model not adequate enough to describe the data in these kinematics.

Figures 3 to 6 show the results of these fits in which both the effective cross section σ and slope factor B were free parameters. The plane-wave calculations generally show little dependence on the spectator angle, in clear disagreement with the change seen in the data. The calculations including FSI manage fairly well to describe the data over the covered kinematics. When comparing the three off-shell descriptions, we see that differences between the three become smaller with higher spectator momentum. This indicates the diminished importance of the off-shell part of the rescattering amplitude in these kinematics.

At the lowest missing momentum of $p_s = 300$ MeV, there is an oscillating structure in the data which disappears for high W but is still present in the calculations. When comparing the three calculations including FSI, we see that there is a large difference between them in the backward angles. There, the no off-shell FSI calculation is smaller than the plane-wave calculations while the maximal off-shell FSI calculation becomes significantly bigger. The fitted off-shell FSI calculations sits somewhere in between and tends to agree more with the maximal off-shell FSI calculation at low W and with the no off-shell one at high W. At this

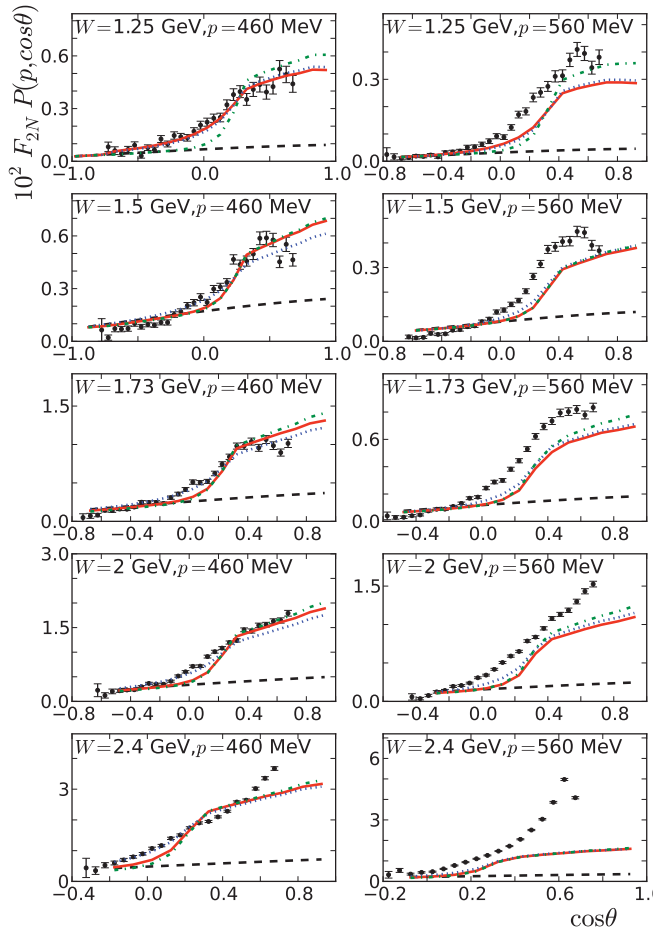

FIG. 6. (Color online) Comparison between the Deeps data [4] and model calculations at $Q^2 = 2.8$ GeV^2 at measured values of invariant mass W and spectator momenta p ($\equiv p_s$ in the text) of 300, 340, and 390 MeV. Graphs as in Fig. 3.

value of spectator momentum, the plane-wave and final-state interaction amplitudes are of comparable magnitudes.[3] This makes the final result quite sensitive to small variations in the FSI amplitude and its off-shell description, thus providing some way of explaining the larger discrepancy between data and different calculations as compared to higher p_s values.

At higher spectator momenta, the no off-shell FSI calculations more or less exhibit three regimes. At backward angles they almost coincide with the plane-wave calculations. Around 90° they show a steep rise, which flattens out at the forward angles. This agrees with the intuitive picture of final-state rescattering. The maximal off-shell FSI calculations, on the other hand, have a more constant slope for the whole of the spectator momentum range. The calculations with a fitted off-shell FSI description show the best agreement with the data, which is to be expected as they have an extra free parameter. Over the whole of the kinematics they generally agree more with the no off-shell FSI calculations than the maximal off-shell FSI ones, pointing at a largely suppressed off-shell

[3]This situation is similar to the quasielastic ^{2}H$(e, e'N)N$ reaction (see, e.g., Ref. [17]).

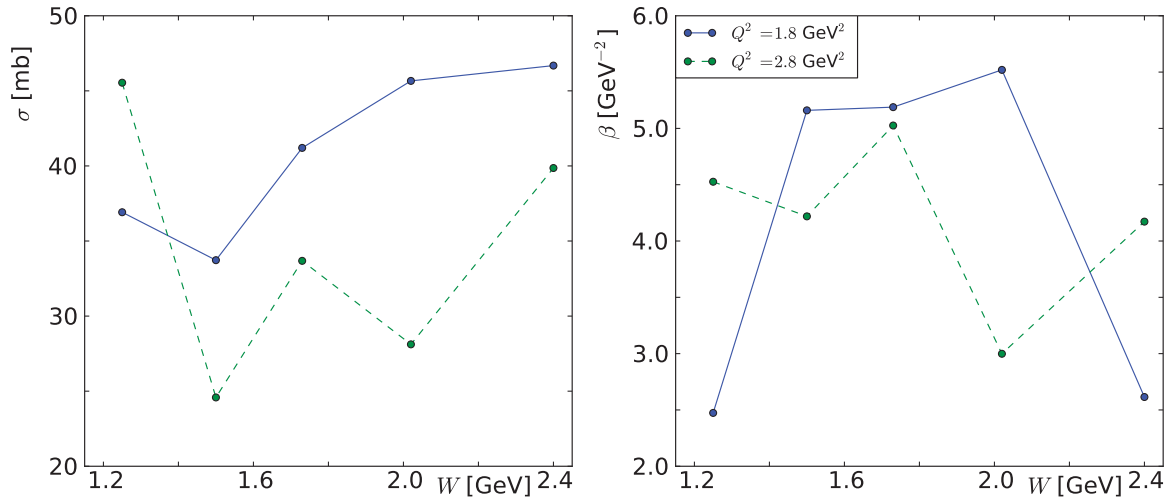

FIG. 7. (Color online) The fitted values of effective cross section σ and slope factor B for the no off-shell FSI calculations used in Figs. 3 to 6 as a function of the invariant mass W. Full blue curve is for $Q^2 = 1.8$ GeV^2, and the dashed green curve is for $Q^2 = 2.8$ GeV^2.

amplitude. At the highest measured spectator momentum the FSI curves systematically underestimate the data, pointing in the direction of a breakdown of the factorization used in this model.

The final question we addressed in the above described fitting procedure is whether the data indicate on Q^2 and W dependence of the parameters of XN rescattering.

Figures 7 and 8 show the values of the fitted parameters $\sigma_{\rm tot}$ and B used in respectively the no off-shell and the maximal off-shell FSI calculations. At $W \approx 1.2$ GeV (corresponding to the production of a Δ), we get a $\sigma_{\rm tot}$ around 40 mb. For the higher invariant masses, the cross section drops to around 20–25 mb and rises with increasing W, consistent with the production of more hadronic constituents in the intermediate state of the DIS reaction. The cross section does not flatten out at the highest W, showing that hadronization occurs before the rescattering in these kinematics. With increasing Q^2, the value of the (XN) cross section parameter also becomes consistently smaller in this region, indicating reduced final-state interactions. This could be a sign of an onset of a color transparency effect, in which with increasing Q^2 the hadronic state is produced in a state with smaller transverse size, subject to reduced QCD interactions with the medium. The values for the slope parameter B are also largely correlated with those of $\sigma_{\rm tot}$ with a smaller slope parameter at higher Q^2 and larger B for higher W, although we also see some clear deviations from this picture (e.g., at $W = 2.4$ GeV in the no off-shell FSI fit). Overall our fitting procedure indicates that the availability of more Q^2 and W data points may allow to gain important insight about the Q^2 and W dependence of the total cross section of NX scattering.

IV. CONCLUSION

Based on the virtual nucleon approximation framework, we developed a model to describe semi-inclusive deep inelastic scattering of the deuteron. To describe the final-state

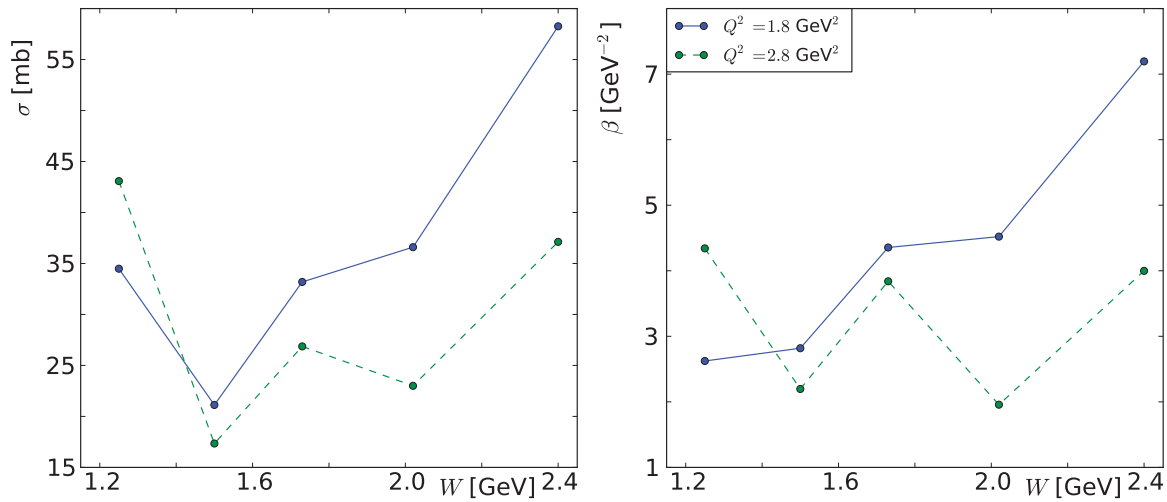

FIG. 8. (Color online) The fitted values of effective cross section σ and slope factor B for the maximal off-shell FSI calculations used in Figs. 3 to 6 as a function of the invariant mass W. Full blue curve is for $Q^2 = 1.8$ GeV^2, and the dashed green curve is for $Q^2 = 2.8$ GeV^2.

interaction of the spectator nucleon with the produced hadronic state X, the general features of diffractive soft rescattering were used, without specifying the structure or space-time evolution of X. The generalized eikonal approximation was used to calculate the scattering amplitudes based on effective Feynman diagram rules. A factorized approach was used to split the cross section into a part describing the virtual photon interaction with the off-shell neutron and a distorted spectral function containing the final-state interactions.

The model calculations were compared to data taken in the Deeps experiment at Jefferson Lab. We first compared our calculation with the data for typical kinematics of the experiment with characteristic parameters for final-state interactions. This comparison indicates a good agreement with the data most importantly describing correctly the rise of FSI in forward direction. This result is opposite to what observed in quasielastic kinematics.

To gain insight on the Q^2 and W evolution of the FSI further calculations were done in which two free parameters (effective cross section σ and slope factor B) in the rescattering amplitude and three different off-shell rescattering prescriptions were considered. Results were fitted for each (Q^2, W) to the available data. The fitted off-shell rescattering parametrizations yielded results similar to the calculations with only an on-shell rescattering amplitude included over a wide range of the kinematics, giving evidence for a largely suppressed off-shell rescattering. The resulting calculations showed reasonable agreement between the data and the calculations including final-state interactions. There were some discrepancies at the highest spectator momentum, which may be caused by the breakdown of the factorization used in the model. At the lowest $p_s = 300$ MeV there is also an oscillating structure in the calculations which is not exactly present in the data at higher W. The calculations in this case proved to be very sensitive to the size of the off-shell amplitude.

When inspecting the values of the parameter fits, three features emerge: (i) The effective cross section rises with increasing W, consistent with the creation of more hadronic constituents taking part in the rescattering. (ii) There is no evidence for a plateau at the highest measured W values, indicating that the hadronic state has hadronized before rescattering takes place. (iii) We obtain lower values for σ_{tot} for the higher Q^2 value, which could be interpreted as a sign of emerging color transparency. However, more data at higher Q^2 are needed to make more definitive statements.

ACKNOWLEDGMENTS

We are thankful to Mark Strikman and Sebastian Kuhn for numerous discussions and useful comments in due course of our study. This work is supported by the Research Foundation Flanders as well as by the U.S. Department of Energy Grant under contract no. DE-FG02-01ER41172.

[1] W. Melnitchouk, M. Sargsian, and M. I. Strikman, Z. Phys. A **359**, 99 (1997).
[2] C. E. Carlson and K. E. Lassila, Phys. Rev. C **51**, 364 (1995).
[3] C. E. Carlson, J. Hanlon, and K. E. Lassila, Phys. Rev. D **63**, 117301 (2001).
[4] A. V. Klimenko *et al.* (CLAS Collaboration), Phys. Rev. C **73**, 035212 (2006).
[5] H. Fenker, C. Keppel, S. Kuhn, and W. Melnitchouk (2003), Report no. jLAB-PR-03-012, [http://jlab.org/exp_prog/CEBAF_EXP/E03012.html].
[6] S. Simula, Phys. Lett. B **387**, 245 (1996).
[7] M. Sargsian and M. Strikman, Phys. Lett. B **639**, 223 (2006).
[8] C. Ciofi degli Atti, L. P. Kaptari, and S. Scopetta, Eur. Phys. J. A **5**, 191 (1999).
[9] C. Ciofi degli Atti and B. Z. Kopeliovich, Eur. Phys. J. A **17**, 133 (2003).
[10] C. Ciofi degli Atti, L. P. Kaptari, and B. Z. Kopeliovich, Eur. Phys. J. A **19**, 145 (2004).
[11] V. Palli, C. Ciofi degli Atti, L. P. Kaptari, C. B. Mezzetti, and M. Alvioli, Phys. Rev. C **80**, 054610 (2009).
[12] C. Ciofi degli Atti and L. P. Kaptari, Phys. Rev. C **83**, 044602 (2011).
[13] L. L. Frankfurt, W. R. Greenberg, G. A. Miller, M. M. Sargsian, and M. I. Strikman, Z. Phys. A **352**, 97 (1995).
[14] L. L. Frankfurt, M. M. Sargsian, and M. I. Strikman, Phys. Rev. C **56**, 1124 (1997).
[15] M. M. Sargsian, Int. J. Mod. Phys. E **10**, 405 (2001).
[16] M. M. Sargsian, S. Simula, and M. I. Strikman, Phys. Rev. C **66**, 024001 (2002).
[17] M. M. Sargsian, Phys. Rev. C **82**, 014612 (2010).
[18] M. M. Sargsian *et al.*, J. Phys. G **29**, R1 (2003).
[19] L. L. Frankfurt and M. I. Strikman, Phys. Rep. **76**, 215 (1981).
[20] L. L. Frankfurt and M. I. Strikman, Phys. Lett. B **64**, 433 (1976).
[21] L. L. Frankfurt and M. I. Strikman, Phys. Lett. B **183**, 254 (1987).
[22] P. V. Landshoff and J. C. Polkinghorne, Phys. Rev. D **18**, 153 (1978).
[23] G. R. Farrar, H. Liu, L. L. Frankfurt, and M. I. Strikman, Phys. Rev. Lett. **61**, 686 (1988).
[24] L. L. Frankfurt, G. A. Miller, and M. Strikman, Annu. Rev. Nucl. Part. Sci. **44**, 501 (1994).
[25] L. Frankfurt *et al.*, Nucl. Phys. A **622**, 511 (1997).
[26] W. Cosyn, M. C. Martinez, and J. Ryckebusch, Phys. Rev. C **77**, 034602 (2008).
[27] J. Ryckebusch, W. Cosyn, B. Van Overmeire, and C. Martinez, Eur. Phys. J. A **31**, 585 (2007).
[28] K. Gallmeister, M. Kaskulov, and U. Mosel, Phys. Rev. C **83**, 015201 (2011).
[29] L. Frankfurt, W. R. Greenberg, G. A. Miller, and M. Strikman, Phys. Rev. C **46**, 2547 (1992).
[30] S. Jeschonnek, Phys. Rev. C **63**, 034609 (2001).
[31] V. N. Gribov, Sov. Phys. JETP **30**, 709 (1970).
[32] L. Bertocchi, Il Nuovo Cimento A **11**, 45 (1972).
[33] R. Machleidt, Phys. Rev. C **63**, 024001 (2001).
[34] M. Lacombe, B. Loiseau, J. M. Richard, R. Vinh Mau, J. Conte, P. Pires, and R. deTourreil, Phys. Rev. C **21**, 861 (1980).
[35] A. Bodek, M. Breidenbach, D. L. Dubin, J. E. Elias, J. I. Friedman, H. W. Kendall, J. S. Poucher, E. M. Riordan, M. R. Sogard, D. H. Coward, *et al.* Phys. Rev. D **20**, 1471 (1979).
[36] L. Frankfurt, M. Sargsian, and M. Strikman, Int. J. Mod. Phys. A **23**, 2991 (2008).